AD-A092 089   COLD REGIONS RESEARCH AND ENGINEERING LAB HANOVER NH   F/G 8/12
              INVESTIGATIONS OF SEA ICE ANISOTROPY, ELECTROMAGNETIC PROPERTIE--ETC(U
              SEP 80   A KOVACS, R M MOREY
UNCLASSIFIED CRREL-80-20   NL

END
DATE
FILMED
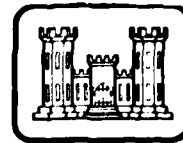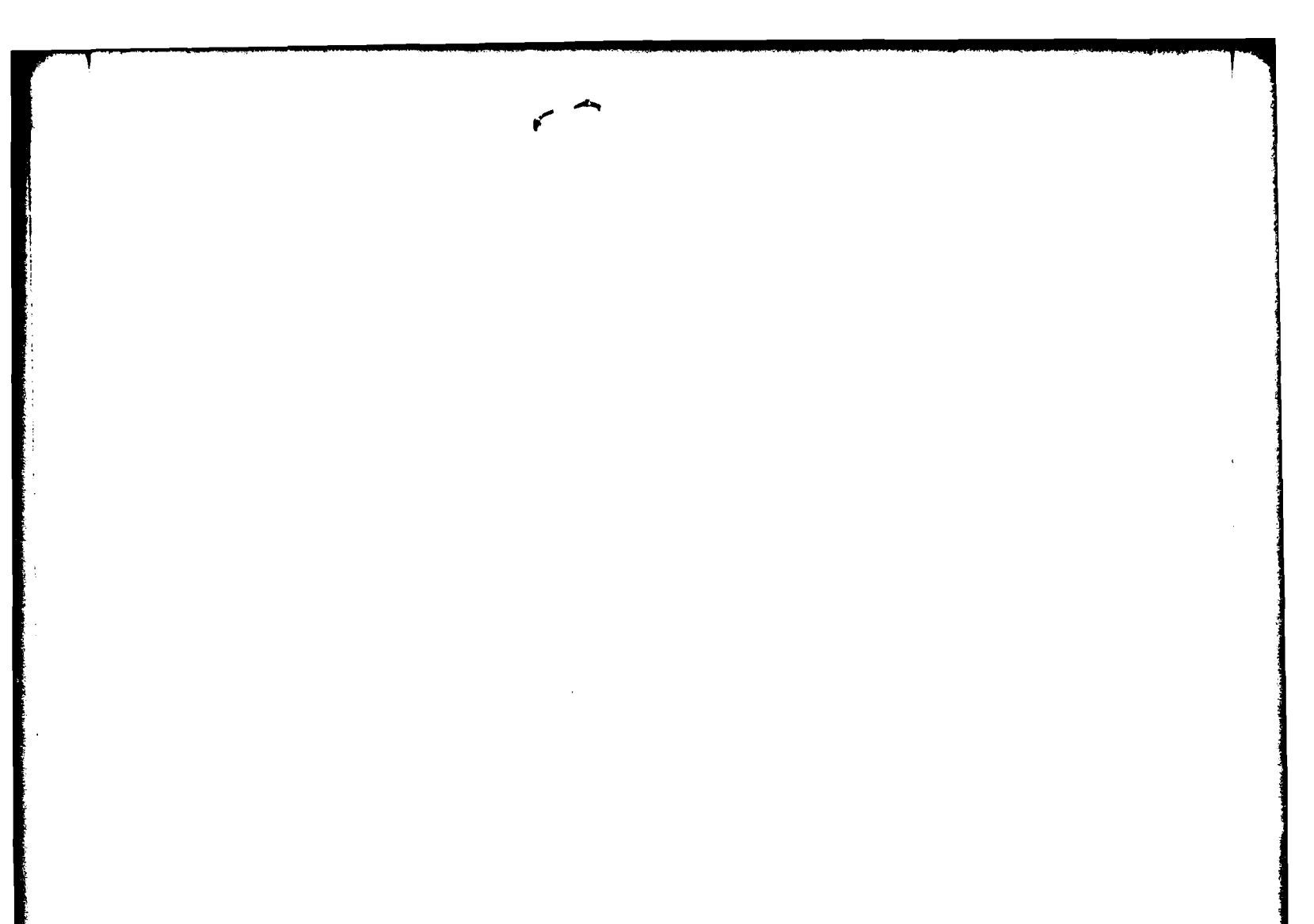81-2
DTIC

CRREL

REPORT 80-20

Investigations of sea ice anisotropy, electromagnetic properties, strength, and under-ice current orientation

DTIC
ELECTED
NOV 6 1980

Axis
x. Refl.

270°

90°

180°

80 007

*Cover: Example of sea ice crystal structure and related
voltage amplitude anisotropy as determined by
radio echo sounding measurements. The light-
toned speckling in the photograph shows where
brine pockets are situated between the 1-mm-
wide ice platelets that compose an ice crystal.
Individual ice crystals are quite irregular and
are represented in this thin section by different
shades of gray. Thin section diameter ~7.5 cm.*

CRREL-80-20

Investigations of sea ice anisotropy, electromagnetic properties, strength, and under-ice current orientation

Austin Kovacs and Rexford M. Morey

Sep 80

26

037100

REPORT DOCUMENTATION PAGE		READ INSTRUCTIONS BEFORE COMPLETING FORM
1. REPORT NUMBER CRREL Report 80-20	2. GOVT ACCESSION NO. AD-A092 089	3. RECIPIENT'S CATALOG NUMBER
4. TITLE (and Subtitle) INVESTIGATIONS OF SEA ICE ANISOTROPY, ELECTROMAGNETIC PROPERTIES, STRENGTH, AND UNDER-ICE CURRENT ORIENTATION		5. TYPE OF REPORT & PERIOD COVERED
		6. PERFORMING ORG. REPORT NUMBER
7. AUTHOR(s) Austin Kovacs and Rexford M. Morey		8. CONTRACT OR GRANT NUMBER(s) ONR Project NR 307-393 NOAA R.D. No. RK-8-0065
9. PERFORMING ORGANIZATION NAME AND ADDRESS U.S. Army Cold Regions Research and Engineering Laboratory Hanover, New Hampshire 03755		10. PROGRAM ELEMENT, PROJECT, TASK AREA & WORK UNIT NUMBERS
11. CONTROLLING OFFICE NAME AND ADDRESS U.S. Navy, Office of Naval Research and U.S. Dept. of Commerce, National Oceanic & Atmospheric Administration		12. REPORT DATE September 1980
		13. NUMBER OF PAGES 23
14. MONITORING AGENCY NAME & ADDRESS(if different from Controlling Office)		15. SECURITY CLASS. (of this report) Unclassified
		15a. DECLASSIFICATION/DOWNGRADING SCHEDULE

16. DISTRIBUTION STATEMENT (of this Report)

Approved for public release; distribution unlimited.

17. DISTRIBUTION STATEMENT (of the abstract entered in Block 20, if different from Report)

18. SUPPLEMENTARY NOTES

19. KEY WORDS (Continue on reverse side if necessary and identify by block number)

Anisotropy.
Arctic regions
Electromagnetic properties
Ocean currents
Sea ice
Strength (mechanics)

20. ABSTRACT (Continue on reverse side if necessary and identify by block number)

Results of impulse radar studies of sea ice give support to the concept of a sea ice model in which the ice bottom is composed of an array of lossy parallel plate waveguides. The fundametal relation between the average bulk brine volume of sea ice and its electrical and strength properties is discussed as is the remote detection of under-ice current alignment. It was found that 1) the average effective bulk dielectric constant is dependent upon the average bulk brine volume of the sea ice; 2) sea ice anisotropy, arising from a bottom structure of crystal platelets with a preferred c-axis horizontal alignment, can be detected by radio echo sounding measurements made not only on the ice surface but also from an airborne platform; 3) the effective coefficient of reflection from the sea ice bottom decreases with increasing average effective bulk dielectric constant of the ice, decreases with increasing bulk brine volume, and is typically one to

DD FORM 1 JAN 73 1473 EDITION OF 1 NOV 65 IS OBSOLETE

11. Controlling Office Name and Address (cont'd)

U.S. Navy		U.S. Department of Commerce
Office of Naval Research		National Oceanic and Atmospheric Administration
Arctic Program	and	OCS Arctic Project Office
800 North Quincy		University of Alaska
Arlington, VA 20390		Fairbanks, AK 99701

20. Abstract (cont'd).

two orders of magnitude lower than the coefficient of reflection from the ice surface; and 4) the losses in sea ice increase with increasing average bulk brine volume.

PREFACE

iii

CONTENTS

ILLUSTRATIONS

TABLES

INVESTIGATIONS OF SEA ICE ANISOTROPY, ELECTROMAGNETIC PROPERTIES, STRENGTH, AND UNDER-ICE CURRENT ORIENTATION

Austin Kovacs and Rexford M. Morey

INTRODUCTION

The *in situ* electromagnetic (EM) properties of sea ice are important in developing instrumentation for the remote sensing of ice thickness and, indirectly, current orientation at the ice/water interface. Studies using an impulse radar sounding system were made in the spring in 1976 and 1977 (Kovacs and Morey 1978) and in 1978 (Kovacs and Morey 1979a) on the sea ice in the area of Prudhoe Bay, Alaska. In these studies it was found that when the crystal structure at the bottom of sea ice had a horizontal c-axis with a preferred azimuthal orientation, this alignment was for all intents and purposes parallel with the short-term (minutes) under-ice current measurements made at the time.

It was observed that this oriented structure behaved as an effective polarizer of transverse electromagnetic waves. The resulting effect was shown to reduce or eliminate the EM signal reflection from the ice bottom when the antenna E-field was oriented perpendicular to the preferred c-axis direction of the ice crystal platelets. But when the E-field was oriented parallel with the preferred crystal c-axis direction a strong signal return was recorded.

It was also found, in sea ice having a highly ordered crystal structure in which the crystals have a preferred horizontal c-axis alignment, that: a) the frequency spectrum of the signal reflected from the ice bottom varied in the horizontal plane, b) the frequency shift was found to be related to the ice brine volume, c) the relative change in bulk dielectric constant versus azimuthal angle did not correlate with the coefficient of anisotropy (in other words *a travel-time anisotropy was not measured, only a reflection anisotropy*), and

d) the surface of the sea ice had no definite anisotropic trend as determined from EM reflection measurements.

This paper extends the previous studies on the EM properties of sea ice as determined with an impulse radar sounding system operating on the ice surface and from an airborne platform, i.e. a helicopter. The field study was made in March 1979, in the area of Prudhoe Bay, at the sites shown in Figure 1.

FIELD PROGRAM

During the April 1978 field program, electromagnetic sounding measurements of sea ice were made using an impulse radar sounding system which radiated a time domain wavelet of about 14 ns duration. The center frequency of the spectrum of the wavelet radiated from the linearly polarized broadband antenna was about 125 MHz, with the -3 db points of the spectrum at about 75 and 150 MHz. This antenna was used as both transmitter and receiver. In March 1979, measurements were made using linearly polarized antennas with a center frequency of the spectrum of the radiated wavelet of about 280 MHz, with the -3 db points of the spectrum at about 220 and 350 MHz. One antenna was used for transmission and one as a receiver. The radiated time domain wavelet was about 6 ns in duration. Both antennas were enclosed in one housing; the distance between the centers of the dipole antennas was about 30 cm.

As in previous studies, radar measurements were made with the radar antenna resting on the ice surface and also with the antenna elevated approximately 1.7 m above the ice surface. In addition, measurements
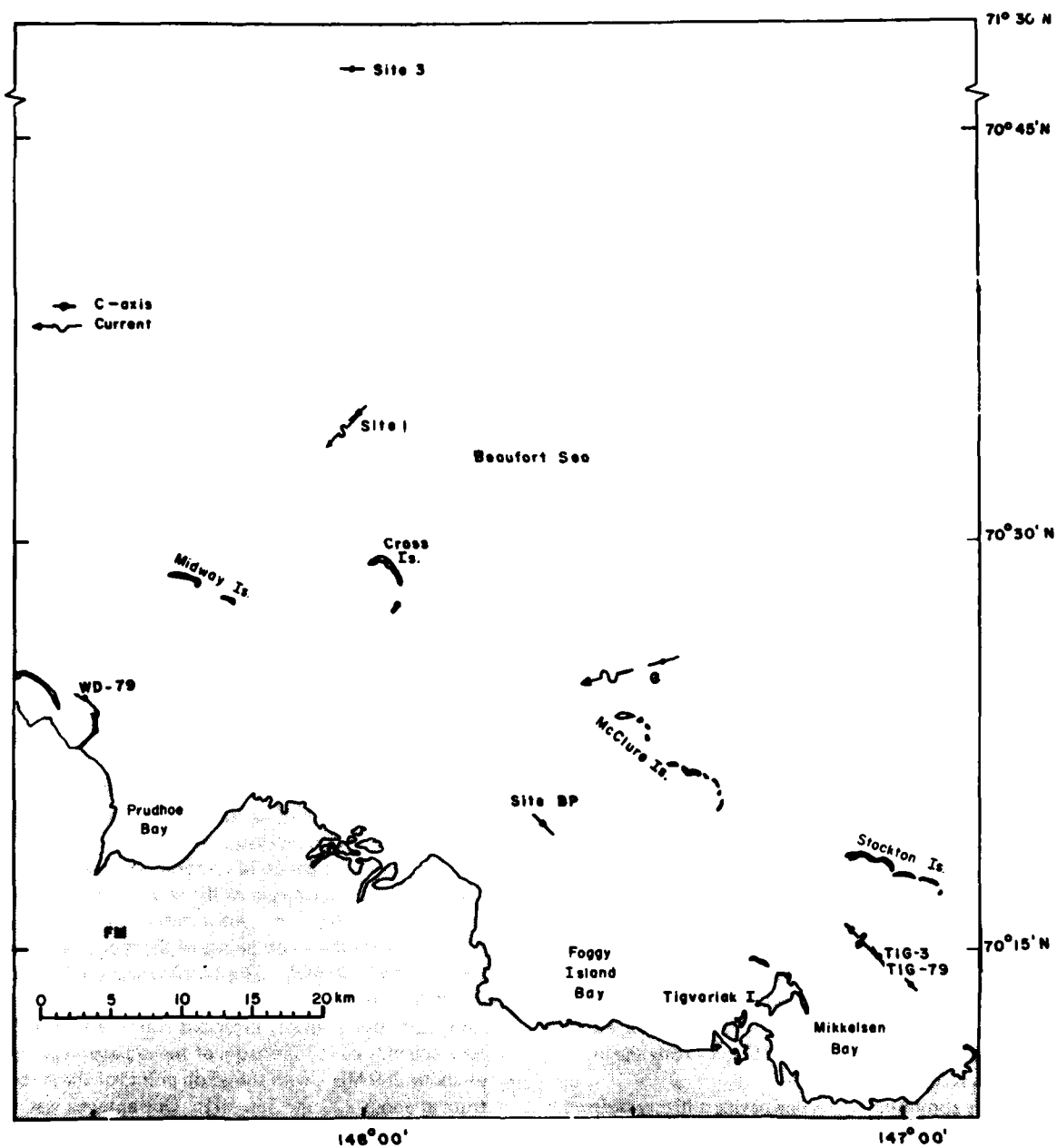
Figure 1. Map of 1977–1979 impulse radar studies. Sites 1, 2 and Tig were 1977 or 1978 study locations. Site G was a study location in 1977, 1978 and 1979. Sites WD-79, BP, Tig 79 and FW were also study locations in 1979.

2

were made with antennas mounted on the side of a NOAA (National Oceanic and Atmospheric Administration) helicopter. These measurements were made with the helicopter resting on the ice surface, during which time the antennas were supported approximately 30 cm above the surface, and also while the helicopter was in flight at an altitude of 10 to 15 m.

Radar measurements from the sea ice surface and from the helicopter were made at a site about 1 km north of the Prudhoe Bay West Dock (WD-79). At three other sea ice sites sounding measurements were made with the radar mounted on the helicopter. Measurements were also made on the ice surface of a freshwater lake. At the WD-79 site the measurement procedure consisted of marking a 30° increment polar grid on the ice surface, making the radar measurements at each grid azimuth, and obtaining an ice core from the center of the grid. Ice core temperature was measured to 0.1°C using a thermistor bridge. Measurements were made at the 1-cm and 5-cm depths and at each 10-cm increment below 5 cm. With the use of a conductivity/salinity bridge, the salinity of the ice was later determined from the meltwater of the top 1½ cm of the ice surface and each 10-cm section of the ice core. Visual observation of the ice core at about the 1- and 1½-m depths and at the ice bottom revealed ice crystal structure and c-axis alignment. Preferred c-axis azimuth orientation was determined with the use of a large compass. These determinations are believed to be accurate to within ±10°. Sea ice brine volume was calculated from the ice core temperature and salinity data.

Radar measurements were obtained with the radar antenna elevated 1.7 m above the ice surface, on top of a wooden structure. A 4-m-square metal screen was set on the ice or snow surface under the antenna. The radiated wavelet reflected from the surface of the screen was recorded on magnetic tape and later used to provide a known reference reflection. The screen was then removed and the radar reflections from the snow surface and ice bottom were recorded at each 30° increment on the polar grid. The snow was removed, and the above sequence of measurements repeated. The antenna was then placed on the ice surface and the reflection from the ice bottom recorded, again at the same 30° grid azimuths.

Measurements made with the antennas mounted on the helicopter were made with the helicopter resting on the ice. The radar reflections from the ice surface and bottom were recorded. Additional readings were made at 30° azimuth increments. This was followed by a series of slow, 10-m altitude flights over the same site, during which the radar reflection of the top and bottom of the ice was again recorded along the same compass headings as when the helicopter was sitting on the ice. An ice core obtained at each site was used to determine, by visual inspection and compass measurement, the preferred c-axis azimuth direction at the ice bottom.

From x-y plots (see Appendix) of the average of ten scans, the two-way travel time of the radar signal in the ice and the relative voltage amplitude of the signal reflected at the snow and ice surface and the ice "bottom" were obtained. The effective bulk dielectric constant ϵ of the sea ice was calculated from

$$\epsilon = \left| \frac{tc}{2D} \right|^2 \tag{1}$$

where c = free space electromagnetic signal velocity
D = tape-measured ice thickness minus 5 cm
t = two-way travel time.

Five centimeters was subtracted from the measured ice thickness because at the impulse radar frequency used in this study the electromagnetic boundary at the bottom of growing sea ice has been found to be about this distance above the ice/water interface (Campbell and Orange 1974), i.e. at or just above the open dendritic ice platelet structure found on the bottom of growing sea ice.

The effective wavelet velocity (V_e) in the sea ice was determined from:

$$V_e = \frac{2D}{t} = \frac{c}{\sqrt{\epsilon}} . \tag{2}$$

An analysis of the frequency spectra (see Appendix) and the relative voltage amplitude of the signal reflected from the various interfaces provided additional information about the material being sounded and the nature of the interfaces. The voltage reflection coefficient of the ice surface (ρ_s) was determined by the ratio of the relative peak-to-peak voltage amplitude of the ice surface and metal screen reflections. The apparent dielectric constant (ϵ_r') of the ice surface was then determined from:

$$\epsilon_r' = \left| \frac{1-\rho_s}{1+\rho_s} \right|^2 . \tag{3}$$

The effective voltage reflection coefficient of the ice bottom (ρ_b) was likewise determined, then corrected for the partial reflection of the energy at the air/ice interface, using:

$$\rho_b' = \rho_b(1-\rho_s^2) \tag{4}$$

3

Table I. Sea ice property and radar reflection analysis determination (snow-free ice).

Site	Ice thick. (m)	Dir.	Ice surface—Antenna elevated Reflection Amp. (V)	Coef. (ρ₀)	Diel. const. (εₛ)	Max. refl. dir.	Refl. anisotropy (K)	Dir.	Ice bottom—Antenna elevated Reflection Amp. (V)	Coef. (ρᵦ)	Diel. const. (ε)	Signal vel. (m/ns)	Max. refl. dir.	Refl. anisotropy (K)	Dir.	Ice bottom—Antenna on ice Reflection Amp. (V)	Diel. const. (ε)	Signal vel. (m/ns)	Max. refl. dir.	Refl. anisotropy (K)	C-axis dir.
WD-79	1.69	0°	3.79	−0.275	3.1			0°	0.27	−0.018	4.6	0.139			0°	1.12	4.9	0.136			
		30	3.43	−0.249	2.8			30	—	—	—	—			30	0.61	5.0	0.134			
		60	3.52	−0.255	2.8			60	—	—	—	—			60	0.66	4.7	0.138	130°	3.4	125°
		90	3.03	−0.278	3.1	None	None	90	0.30	−0.020	4.7	0.138	133°	2.0	90	1.32	4.5	0.141			
		120	3.71	−0.269	3.0			120	0.54	−0.037	4.5	0.142			120	1.82	4.7	0.139			
		150	3.58	−0.260	2.9			150	0.41	−0.028	4.5	0.142			150	1.68	4.7	0.138			
		Avg.		−0.264	3.0			Avg.		−0.026	4.6	0.140			Avg.		4.6	0.138			
1	1.60	0	5.38	−0.252	2.8			0	0.33	−0.002	6.4	0.118			0	0.31	—	—			
		30	5.44	−0.255	2.8			30	0.52	−0.004	6.7	0.116			30	0.50	—	—			
		60	5.64	−0.265	3.0	100°	1.1	60	0.08	−0.001	6.5	0.117	42	13.6	60	0.56	6.7	0.116	46	8.1	40
		90	6.12	−0.290	3.3			90	0.28	−0.002	6.9	0.115			90	0.33	6.4	0.118			
		120	5.79	−0.272	3.1			120	0.16	−0.001	6.4	0.118			120	0.25	6.2	0.120			
		150	5.79	−0.272	3.1			150	0.09	−0.001	6.2	0.120			150	0.12	6.4	0.118			
		Avg.		−0.268	3.0			Avg.		−0.002	6.5	0.117			Avg.		6.4	0.118			
3	1.83	0	2.70	−0.226	2.5			0	—	—	—	—			0	0.23	5.7	0.125			
		30	3.01	−0.249	2.8			30	0.20	−0.002	5.2	0.132			30	0.76	5.0	0.134			
		60	3.36	−0.277	3.1	70	1.2	60	0.54	−0.004	5.2	0.131	80	4.8	60	0.71	5.1	0.133	80	15.0	90
		90	3.23	−0.266	3.0			90	0.75	−0.006	5.2	0.129			90	1.55	5.2	0.132			
		120	2.99	−0.247	2.7			120	0.41	−0.003	5.5	0.128			120	0.83	5.1	0.133			
		150	2.47	−0.204	2.3			150	0.17	−0.001	5.9	0.123			150	0.20	5.6	0.127			
		Avg.		−0.244	2.7			Avg.		−0.003	5.4	0.129			Avg.		5.3	0.131			
FW	2.01	0	2.65	−0.284	3.2			0	2.11	−0.208	3.1	0.170			0	5.41	3.1	0.170			
		90	2.52	−0.270	3.0	—	—	90	2.05	−0.204	3.1	0.170	—	—	90	5.49	3.1	0.170	—	—	—
		Avg.		−0.277	3.1			Avg.		−0.206	3.1	0.170			Avg.		3.1	0.170			

4

Table II. Sea ice property and radar reflection analysis determination (snow-covered ice).

Site	Ice thick. (m)	Snow/Ice surface — Antenna elevated Reflection Dir.	Amp. (V)	Coef. (ρ_s)	Diel. const. (ε_i)	Max. refl. dir.	Refl. aniso-tropy (K)	Ice bottom — Antenna elevated Reflection Dir.	Amp. (V)	Coef. (ρ_b)	Diel. const. (ε)	Signal vel. (m/ns)	Max. refl. dir.	Refl. aniso-tropy (K)	C-axis dir.	Snow thick. (cm)
WD-79	1.69	0°	3.73	-0.271	3.0			0°	0.24	-0.016	4.6	0.139				
		30	3.22	-0.234	2.6			30	–	–	–	–				
		60	2.98	-0.216	2.4	None	None	60	–	–	–	–	131°	2.4	125°	3.5
		90	3.76	-0.272	3.0			90	0.26	-0.017	4.8	0.137				
		120	3.33	-0.242	2.7			120	0.45	-0.031	4.5	0.141				
		150	3.12	-0.232	2.6			150	0.38	-0.026	4.6	0.140				
		Avg.		-0.245	2.7			Avg.		-0.023	4.6	0.139				

Table III. Site average bulk brine volume and minimum effective electromagnetic propagation losses.

Site	Avg. brine vol. (‰)	Min. two-way loss (db)	Ice/water interface loss (db)	Spreading loss (db)	Min. two-way A + S losses (db)	Min. one-way A + S losses (db/m)
WD-79	47	-29 @ 120°	-7	-6	-16	-5
1	76	-48 @ 30°	-7	-6	-35	-11
3	66	-43 @ 90°	-7	-7	-29	-8
FW	0	14	-3.5	-7	-3.5	-0.87

where ρ'_b is the corrected effective voltage reflection coefficient. This coefficient includes losses due to geometric spreading, attenuation, and interface effects. As a check on the measured reflection coefficient ρ_s for the lake ice, the theoretical voltage reflection coefficient at the air/ice interface ($R_{a/i}$) was calculated from:

$$R_{a/i} = \frac{\sqrt{\epsilon_i/\epsilon_a} - 1}{\sqrt{\epsilon_i/\epsilon_a} + 1} \tag{5}$$

where ϵ_i and ϵ_a are the dielectric constants for the ice surface and air, respectively.

Similarly, the theoretical voltage reflection coefficient at the ice/water interface was determined from:

$$R_{i/w} = \frac{\sqrt{\epsilon_w/\epsilon_i} - 1}{\sqrt{\epsilon_w/\epsilon_i} + 1} \tag{6}$$

where ϵ_w is the dielectric constant of fresh water.

Reflection coefficients ρ_s and ρ'_b were used to calculate signal losses at the ice surface and ice bottom in db using:

$$|\rho| \ (db) = 20 \log_{10}|\rho|. \tag{7}$$

Finally, the center frequency of the spectrum of the time-amplitude wavelet reflected from the metal screen, the snow and ice surfaces and the ice bottom was determined using a digital signal analyzer (see Appendix).

RESULTS AND DISCUSSION

Radar reflection results for the Prudhoe Bay West Dock sea ice site in 1979 (WD-79) and for the freshwater lake ice site (FW) are listed in Tables I–III, along with similar sea ice results for sites 1 and 3 studied in 1978 (Kovacs and Morey 1979a). In addition, the WD-79 data are presented on polar coordinate plots from which a coefficient of anisotropy (K) is obtained, as determined by the ratio of the major-to-minor axis of the polar plot of the wavelet reflection amplitudes vs E-field azimuth (see, for example, Figure 5).

When the antenna was elevated, the reflection amplitude of the signal from the snow and ice surface changed slightly with antenna E-field azimuth orientation. These small variations indicated no near-surface preferred crystal orientation, and therefore no anisotropy (Fig. 2a and 2b). This was further verified by our
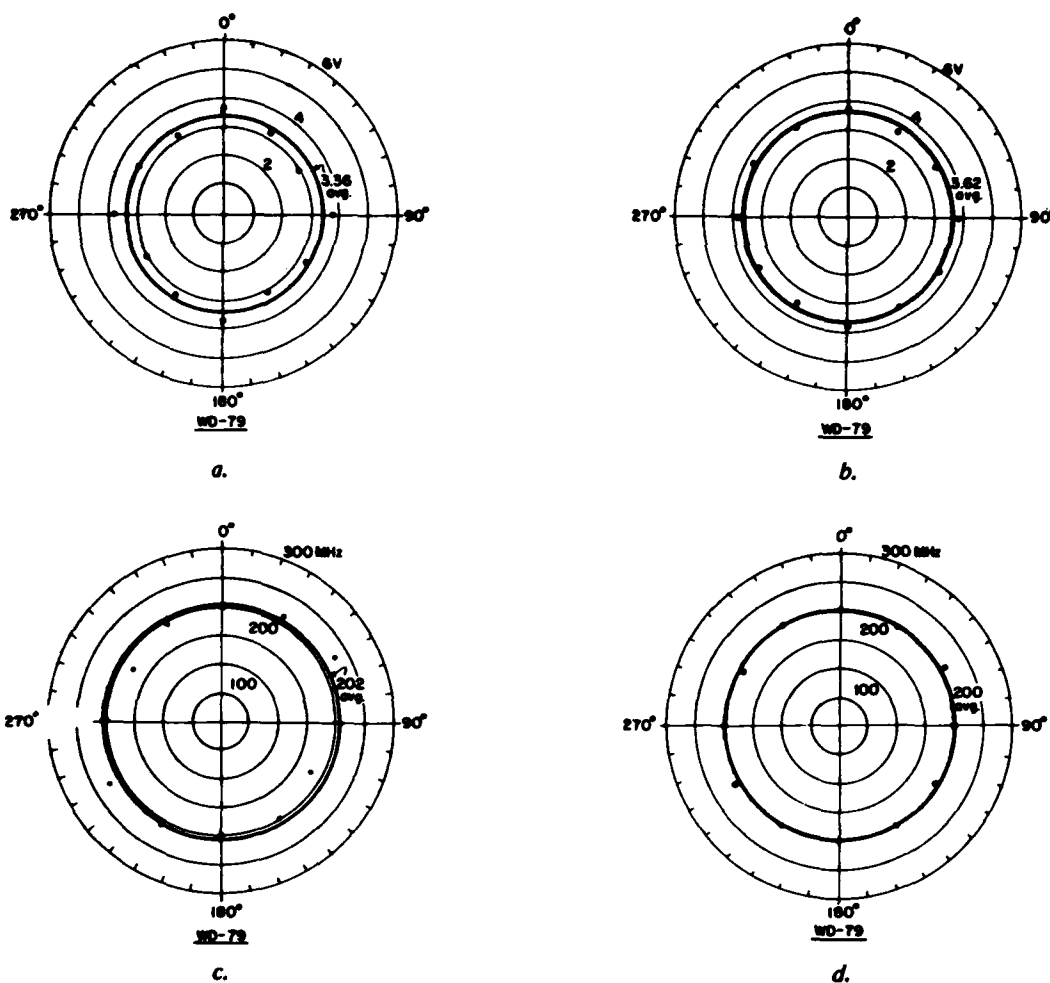
5

Figure 2. *Relative voltage amplitude of reflected wavelet from the snow (a) and ice (b) surfaces, and the center frequency of the spectrum of the reflected signal from the snow (c) and ice (d) surfaces when the antenna was elevated at site WD-79.*

visual inspection of the ice surface crystal structure and by more detailed petrographic studies of sea ice by many other investigators, e.g. Langhorne (in press) and Weeks and Gow (1979). Similarly, polar plots of center frequency vs E-field azimuth orientation do not exhibit any frequency shift (Fig. 2c and 2d). These results agree with those of Kovacs and Morey (1978), who found that "all data gathered to date using impulse radar indicate that the surface of sea ice is either not anisotropic in the horizontal plane or only weakly anisotropic."

The center frequency of the spectrum of the reflected signal from the metal sheet was found to be about 280 MHz. However, the center frequency of the reflected signal from the snow and ice surfaces shifted down to about 200 MHz, as shown in Figures

2c and 2d. Evidently frequency-dependent absorption effects reduced the amplitude of the higher frequencies in the reflected wavelet. Here, too, the polar plots show that while the center frequency varied slightly vs E-field orientation, there was no preferred azimuthal trend.

The same is true for the center frequency of the wavelet reflected from the ice bottom when the antenna was elevated and when it was resting on the ice surface (Fig. 3a and b). These results indicate that the frequency-dependent properties of sea ice are not dependent upon azimuth direction. However, the results of Kovacs and Morey (1979a) showed a frequency dependence vs E-field azimuth at the lower frequency wavelet spectrum used in their study. We do not fully understand the differences between these two results.
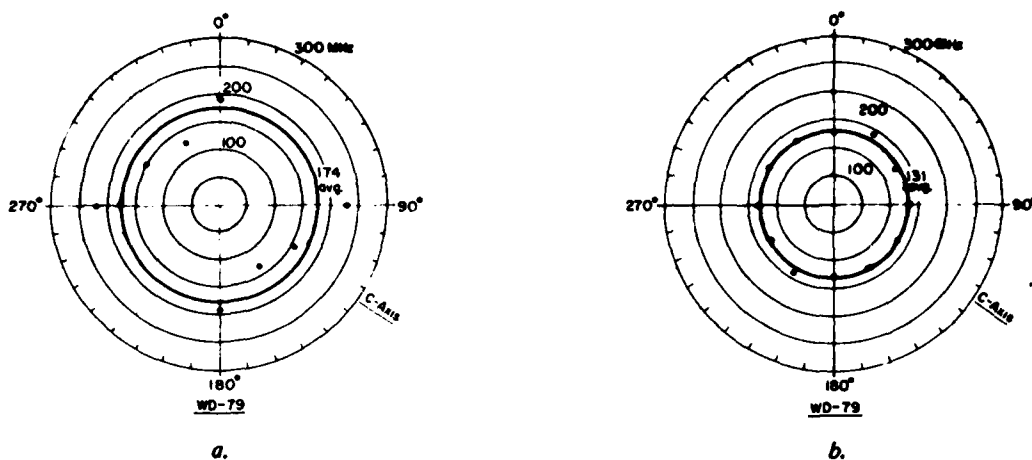
6

Figure 3. C-axis direction and center frequency of the spectrum of the reflected signal from the ice bottom vs antenna E-field azimuth at site WD-79, when the antenna was elevated (a) and when it was resting on the ice surface (b).
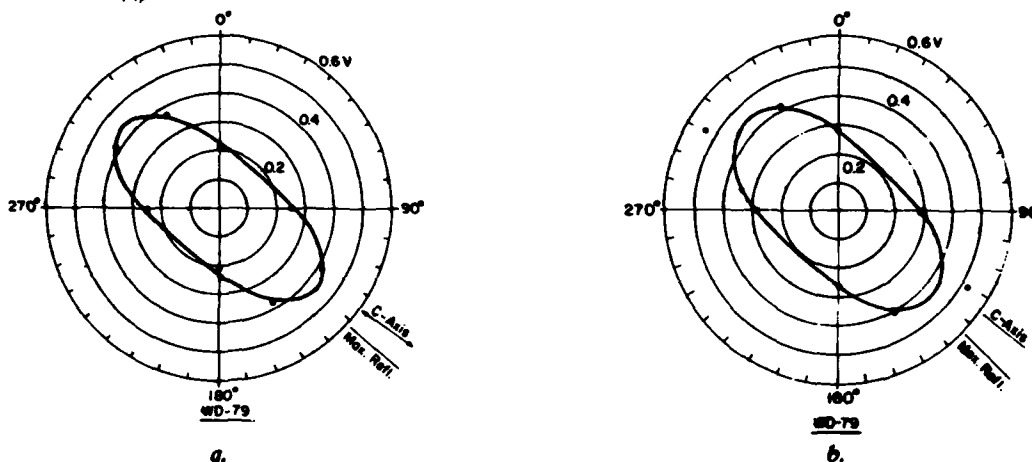

Figure 4. C-axis direction and relative voltage amplitude of the wavelet reflected from the ice bottom vs antenna E-field azimuth at site WD-79, when the antenna was elevated and the ice surface was snow-covered (a) and snow-free (b).

The significant difference between the two plots shown in Figure 3 is the average of the center frequencies of the signal reflected from the ice bottom: 174 MHz when the antenna was elevated and 131 MHz when the antenna was resting on the ice surface. The latter is the result of antenna loading effects which occur when an antenna is brought in contact with another material. When this occurs, the beam pattern and frequency spectrum of the radiated signal are modified.

The relative voltage amplitude of the reflected signal from the ice bottom vs E-field direction when the antenna is elevated is shown in Figures 4a and b. Also shown is the preferred ice bottom crystal c-axis azimuth orientation. The variation in the relative voltage

amplitude vs antenna E-field orientation is striking; it is clear that maximum reflection occurs when the E-field is aligned parallel with the predominant c-axis direction. This is in keeping with earlier findings (Kovacs and Morey 1978, 1979a). In light of such data, it was deduced that the sea ice behaved as an effective polarizer of the radiated electromagnetic energy, and is thus anisotropic. The lack of measurable signal level at the 30–210° and 60–240° azimuth angle precludes construction of an ellipse which may have taken the form of that in Figure 5. However, an apparent coefficient of anisotropy was determined from the ellipse drawn through the available data, as shown in Figures 4a and b. The resulting apparent coefficient of anisotropy is nearly the same (Tables I and II, WD-79,
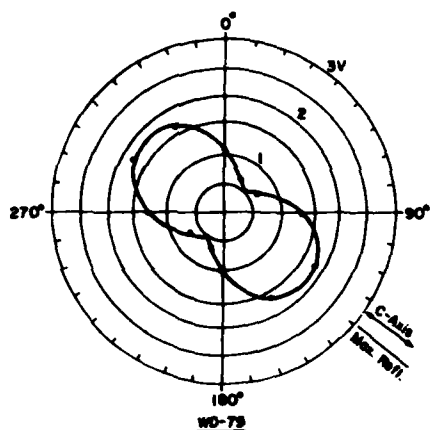
7

Figure 5. *C-axis direction and relative voltage amplitude of the wavelet reflected from the ice bottom vs antenna E-field azimuth at site WD-79, when the antenna was resting on the ice surface.*

antenna elevated), with or without a snow cover on the ice surface: 2.0 and 2.4, respectively. The relative voltage amplitude of the wavelet reflected from the ice bottom was slightly lower when the ice surface was covered with 3½ cm of snow.

The relative voltage amplitude of the reflected signal vs antenna E-field azimuth orientation when the antenna was resting on the ice surface is shown in Figure 5. Again, it is clear that maximum signal reflection amplitude occurs when the antenna E-field is aligned parallel with the preferred c-axis direction.

The last set of radar measurements at the West Dock site was made with two antennas fixed to the NOAA helicopter, as shown in Figure 6a. At this site, only information from one of the two antennas shown mounted to the helicopter was recorded for later analysis. Measurements were made while the helicopter was on the ice surface (Fig. 6a) and in flight (Fig. 6b). The relative voltage amplitude results for the airborne antenna vs those for when the antenna was resting on the ice surface are shown in Figure 7. The agreement between the airborne measurements and the static on-ice measurements is apparent, demonstrating for the first time that it is possible to detect the existence of a preferred c-axis orientation at the "bottom" of sea ice from an airborne platform. Because the c-axes are believed to be aligned with the long-term current direction at the ice/water interface (Kovacs and Morey 1979a, Weeks and Gow 1979, Langhorne, in press), it should be possible to determine, indirectly, this azimuthal alignment from an airborne platform in remote areas.
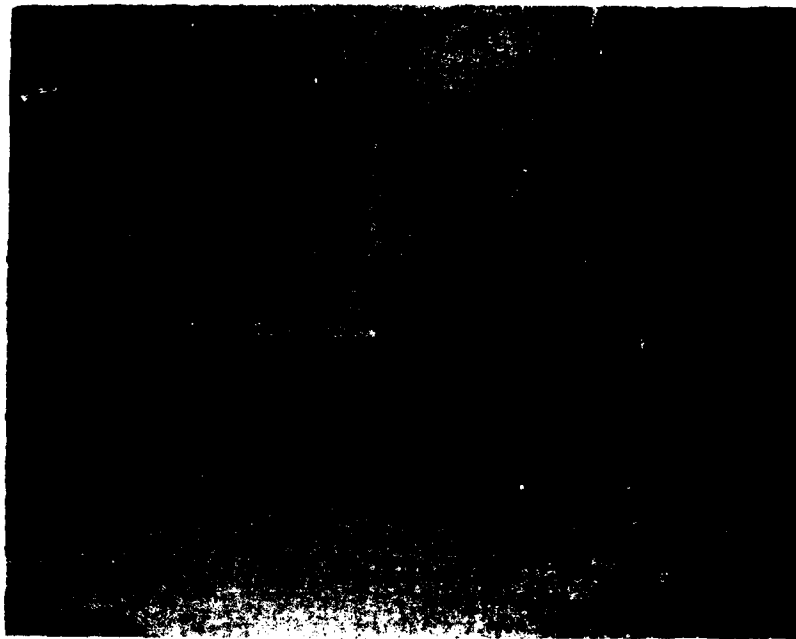
The difference in relative voltage amplitude for the three polar plots shown in Figure 7 is the result of various system gain settings used for each of the measurements. The coefficients of anisotropy of the reflected signal for the antenna resting on the ice sur-

face, mounted on the helicopter with the helicopter on the ice, and airborne are 3.4, 5.2 and 2.5, respectively. These results indicate that the sea ice anisotropy, and therefore the prevailing current alignment at the ice/water interface, may be more difficult to detect from an airborne platform than from the surface.
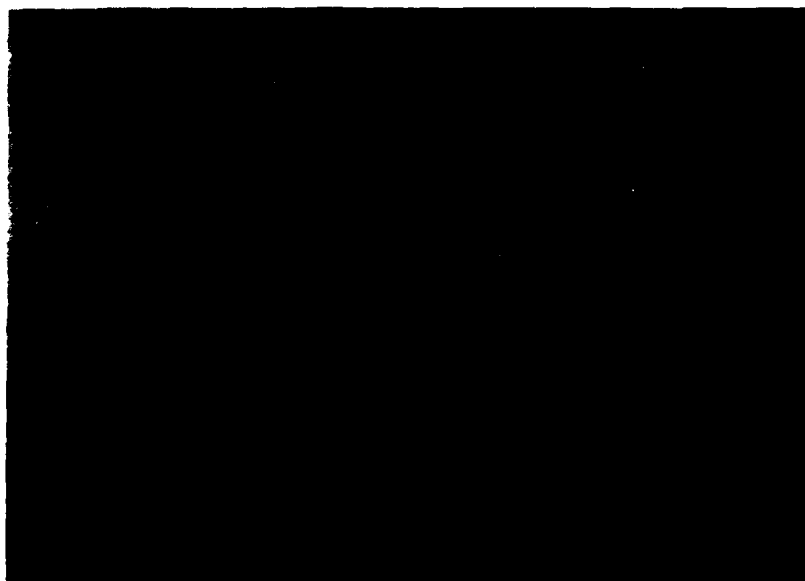
Examples of the impulse radar signal data collected during a helicopter flight and displayed on a graphic recorder are shown in Figures 8a and b. The long period variation in the record is due to gradual changes in helicopter altitude. The radar signatures from the ice surface and bottom when the antenna E-field is flown "parallel" to the preferred c-axis direction are apparent (Fig. 8a). The reflected signal from the ice bottom when the antenna E-field is not aligned with the preferred c-axis alignment is not as apparent (Fig. 8b). As the darkness of the record is a function of the voltage amplitude of the reflected signal, it is clear from the records that the reflected signal strength from the ice bottom in Figure 8b was weaker.

Airborne radar sounding measurements were also made at sites Tig-79, Boulder Patch (BP) and G (Fig. 1). At Tig-79 the ice was covered with 12 cm of snow. Ice thickness was 1.59 m and the local c-axis orientation was 150° true. The direction of maximum reflection amplitude was 154° true (Fig. 9). The ice exhibited a strong coefficient of anisotropy (4.7). Not far from this site, at the 1978 field season location Tig-3 (Fig. 1), the under-ice current was found to be from 130° true (Kovacs and Morey 1979a).

The ice bottom reflection amplitude data from Site BP (shown in Fig. 10) gave a coefficient of anisotropy of 1.4. The direction of maximum signal strength was 135° true, in agreement with the preferred c-axis orientation of the bottom ice, which was found to be 140° true. Snow cover at the site was less than 2 cm. Ice thickness was 1.60 m. Two ice cores from

8

a.

b.

*Figure 6. Configuration of dual antennas mounted to the helicopter during on-ice
(a) and airborne (b) sounding of sea ice. View a also shows emergency field rotor
deicing.*

Figure 7. *C-axis direction and relative voltage amplitude of the wavelet reflected from the ice bottom vs antenna E-field azimuth at site WD-79, when the antenna was airborne, on the ice surface, and mounted to the helicopter approximately 30 cm above the ice surface.*

a.

b.

Figure 8. *Graphic records of airborne impulse radar echo sounding of sea ice. The top return in each record is from the ice surface and the next return is from the ice bottom. The long period variation in the record is due to changing aircraft altitude.*

10

Figure 9. C-axis direction and relative voltage amplitude of the wavelet reflected from the ice bottom vs antenna E-field azimuth at site Tig-79 (antenna airborne).
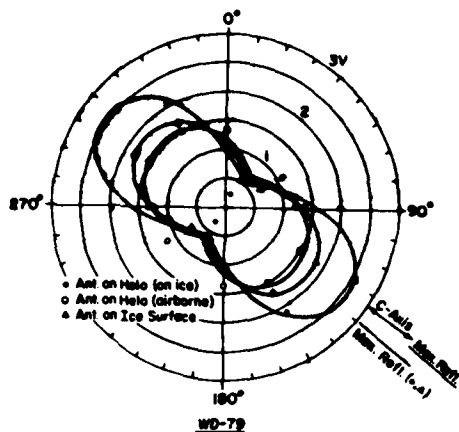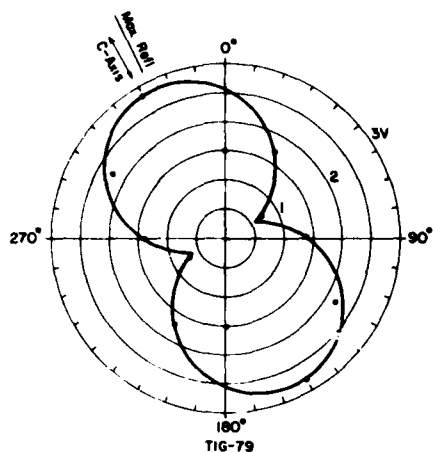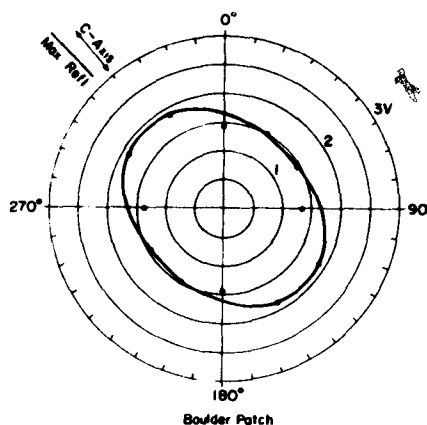

Figure 10. C-axis direction and relative voltage amplitude of the wavelet reflected from the ice bottom vs antenna E-field azimuth at the Boulder Patch site (antenna airborne).

Figure 11. Ice cores obtained at the Boulder Patch site.

this site are shown in Figure 11. The upper three-quarters of the ice was clear; below this was a band of dirty ice not found at other sites studied in 1979, and at the bottom there was another layer of clear ice, about 5 cm thick.

At site G, the snow cover was less than 1 cm thick, the ice was 1.55 m thick and the preferred c-axis orientation was 80° true. In 1977, the current direction at this site was measured and was found to be from 80° true, at 4 cm/s. The c-axis was also found to be oriented at 80° true, which is in agreement with the 1979 determination.

At site G, airborne radar soundings were made from both of the helicopter-mounted antennas. Each antenna was operated independently in the transceive mode. The ice bottom reflection amplitude data are shown in Figure 12. The difference in wavelet amplitude between the two antennas is due, in part, to different gain settings. Both sets of antenna data reveal that the ice is anisotropic, with the maximum reflection occurring

11

Figure 12. C-axis direction and relative voltage amplitude of the wavelet reflected from the ice bottom vs antenna E-field azimuth for when the antenna or antennas were "on" the ice and airborne at site G. From the polar plots it appears that antenna 2 has more directivity then antenna 1.
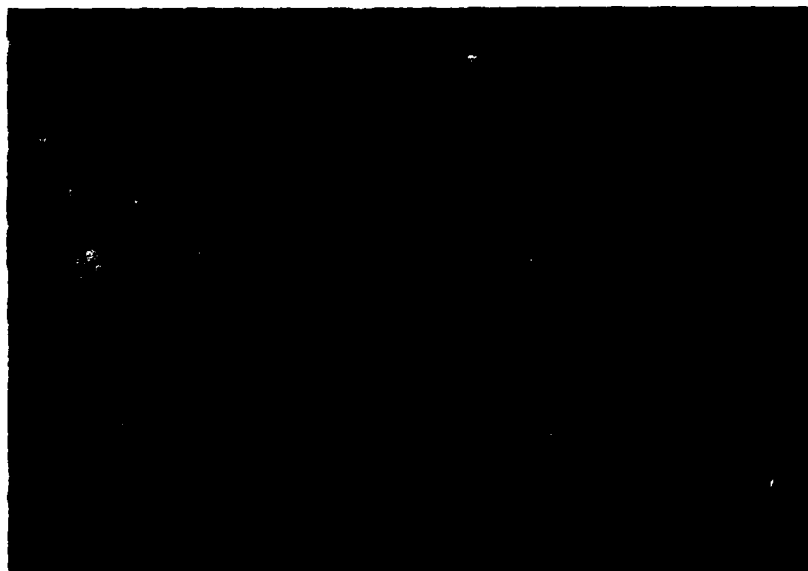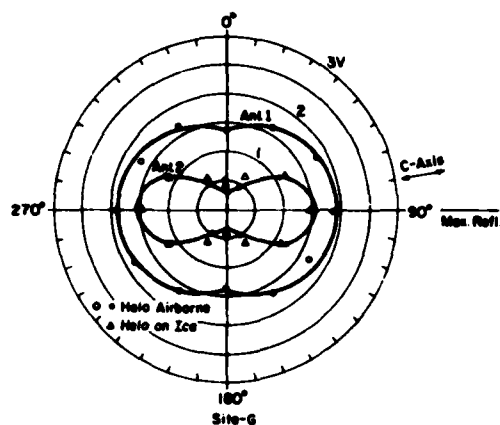
in the same direction, i.e. at 90° true. This is in agreement with local current (Fig. 1) and c-axis direction observations. The latter was again found in 1979 to be at 80° true. Also shown in Figure 12 are the radar sounding data obtained from antenna 2 when the helicopter was rotated on the ice surface. These data are in agreement with the airborne data from the same antenna. The fact that these two sets of data have similar amplitude is a coincidence, as the gain setting was lower during the on-ice measurements than during the airborne measurements.

Our measurements at the freshwater lake site were not intended to detect anisotropy within the ice, but were made for control purposes and as a check to validate the sea ice measurements. However, measurements were made with the antenna E-field oriented at 0 and 90° true. The resulting radar reflection amplitude data are listed in Table I.

From equations previously presented, ice surface and bottom coefficient of reflection, apparent surface and bulk dielectric constants and bulk velocity calculations were made using the radar reflection amplitude and signal flight times vs antenna E-field orientation. These results are listed in Tables I and II for the 1978 West Dock and lake ice sites, along with similar data for sea ice sites 1 and 3, studied in 1978. The latter site information is listed for comparative purposes and because the bottom coefficient of reflection had not previously been determined.

From the elevated antenna data the average surface reflection coefficient for the freshwater lake ice (FW) was determined to be -0.277, from which the apparent dielectric constant is calculated to be 3.12. This is in agreement with accepted published values (3.1 to 3.2) for freshwater ice. The effective velocity and bulk dielectric constant were determined to be 0.170 m/ns and 3.1, respectively. Again, these values are in agreement with accepted published values.

The coefficient of reflection from the lake ice bottom was determined to be -0.206. This value is low in comparison with the theoretical value of -0.684 (calculated from eq 6 using 3.1 for ϵ_i and 88 for ϵ_w). The lower measured value for the coefficient of reflection is believed to be due to beam spreading, signal absorption and scattering (A and S) losses within the lake ice. The A and S losses were calculated and are listed in Table III, along with those for sea ice locations WD-79 and sites 1 and 2. The loss at the "sea ice/water interface" was calculated using 12 for ϵ_i and a relative complex dielectric constant ϵ_w^* of 310 for ϵ_w in eq 6. The relative complex dielectric constant of the seawater was calculated from:

$$\epsilon_w^* = \epsilon_w' + j\epsilon_w'' = \epsilon_w' + j\frac{\sigma}{2\pi f \epsilon_o} \qquad (8)$$

where ϵ_w' = real part of the complex dielectric constant of seawater $\approx$ 88 at -1°C

ϵ_w'' = imaginary part of the complex dielectric constant

σ = conductivity of seawater $\approx$ 3 mhos/m at -1°C

f = frequency (175 MHz from Fig. 3a)

ϵ_o = free space dielectric constant = 8.854x10^{-12} farads/m.

Therefore, $\epsilon_w^* = 88 + j308$ and $|\epsilon_w^*| \approx 310$, which is an approximate value for use in eq 6 to take into account the very high conductivity of seawater. The resulting value for R_i/w is 0.671. Because the electromagnetic boundary at the sea ice bottom has a higher brine volume (Fig. 13), the value selected for ϵ_i is our best estimate at this time. It is based upon the extrapolation of the curve in Figure 14 to a brine volume representative of that found at the bottom of sea ice. Future studies are planned to clarify this.
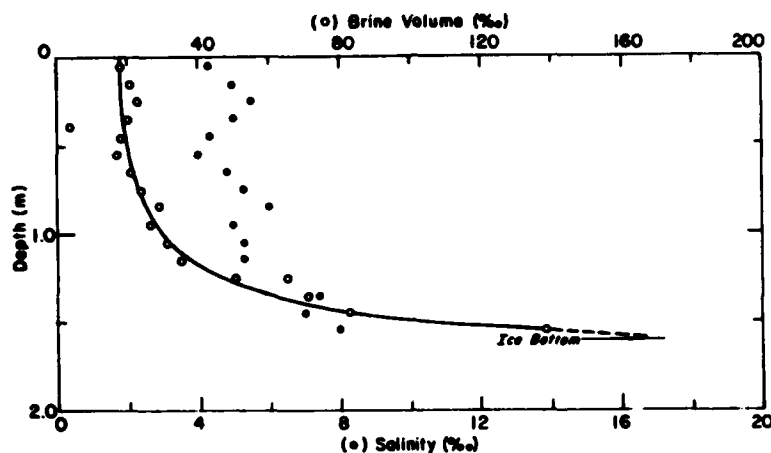
12

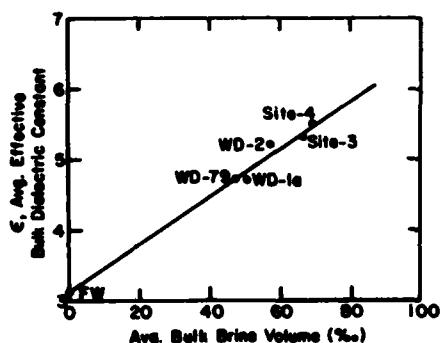Figure 13. Brine volume and salinity distribution vs depth at site WD-79.

Figure 14. Average effective bulk dielectric constant vs average bulk brine volume of ice.

Table IV. Site ice thickness, average bulk brine volume and average dielectric constant.

Site	Ice thick. (m)	Avg. brine vol. (%o)	Avg. diel. const.
WD-79	1.69	47	4.6
1	1.60	76	6.5
3	1.83	66	5.4
FW	2.01	None	3.1

The total two-way transmission losses, total two-way A and S loss and the one-way A and S loss (from Table III) are plotted vs the average bulk brine volume of the ice for each site (Table IV) in Figure 15. These losses were determined from the elevated antenna data and represent the minimum loss which occurred at the maximum recorded voltage amplitude of the signal from the ice bottom. The loss in the sea ice is shown to increase exponentially with increasing average bulk brine volume. It is apparent that when the average bulk brine volume reaches something on the order of $100^o/oo$, A and S losses become very high and will probably prevent the detection of the sea ice bottom. This would apply to the radar system used when it is elevated 1.5 m above the ice surface and to when the antenna E-field is aligned with the preferred c-axis direction of the ice. Since the losses become much larger when the antenna E-field is oriented perpendicu-

lar to the c-axes (because the voltage amplitude of the reflected wavelet from the ice bottom decreases significantly in this direction), it is even more unlikely that the sea ice bottom could be detected with this E-field alignment. For example, at this E-field direction the total two-way losses at Sites WD-79, 1 and 3 become -35, -64 and -60 db, respectively. These values are significantly larger than the losses listed in Table III. The ice bottom might still be detectable if the antenna were resting on the surface, as the spreading losses would be less. Conversely, the higher the antenna is above the ice surface, the lower the average bulk brine volume of the ice need be to prevent "seeing" the ice bottom. Indeed, in the spring of 1978, from an altitude of approximately 15 m, the ice bottom was not detectable at site 1 (Fig. 1), where the ice had an average bulk brine volume of $\sim 76^o/oo$; but the bottom was intermittently detectable at site 3 (Fig. 1), where the
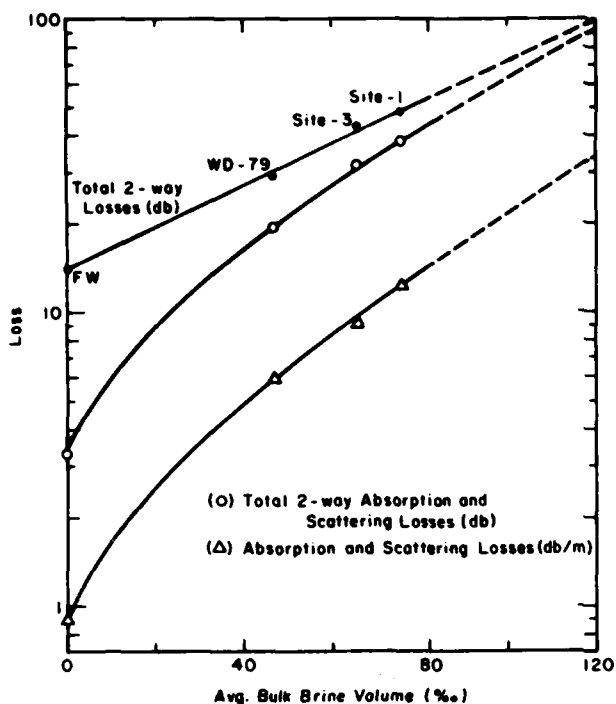
13

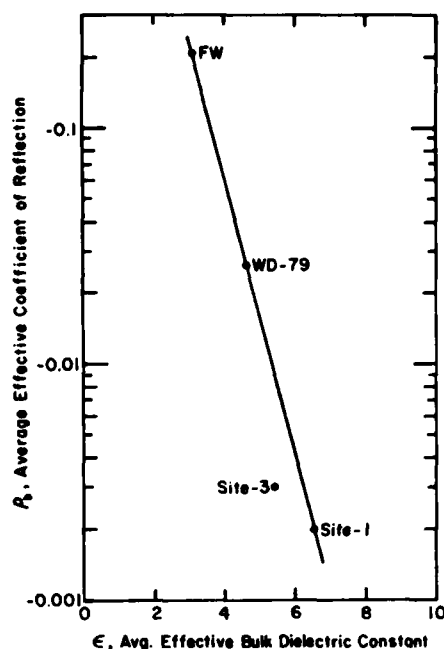Figure 15. Transmission losses in ice vs its average bulk brine volume.

Figure 16. Average effective coefficient of reflection from the ice bottom vs average effective bulk dielectric constant of the ice.
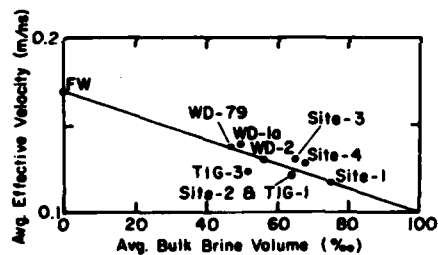

Figure 17. Average effective velocity of the electromagnetic signal in ice vs its average bulk brine volume. The equation for the line passing through the data is $Ve = 0.17 - 0.00068v$ with a correlation coefficient of 0.90.

average brine volume of the ice was on the order of $66^o/_{oo}$.

The average effective coefficient of reflection at the ice bottom for when the antenna is elevated vs average bulk dielectric constant (Table 1) is shown in Figure 16. The average effective coefficient of reflection is shown to become smaller as the average effective bulk dielectric constant increases. This again indicates that the ice is becoming more lossy with increasing brine volume.

Another way of showing this is by the plot of average effective bulk dielectric constant vs average bulk brine volume, as shown in Figure 14. In this graph, ϵ is shown to increase linearly with increasing brine volume. The data presented are from the 1978 field re-

sults of Kovacs and Morey (1979a) and from the 1979 field season for ice over 1.6 m thick. Because of the limited scatter in the data, the second parameter should be easily obtainable from the graph after one parameter is measured.

The data in Figure 14 can be replotted as the average effective velocity vs the average bulk brine volume, using eq 2, as shown in Figure 17. It is shown that the average effective velocity decreases linearly as the average bulk brine volume of the ice increases.

The above findings are significant, for they provide a way to not only measure sea ice thickness, but also to infer its strength remotely from radio echo sounding information. This concept has also been suggested by Rossiter et al. (1977). This may be achieved with the
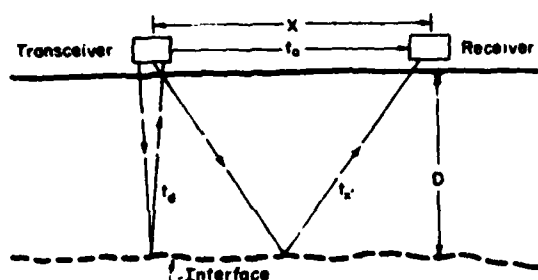
14

Figure 18. Schematic for dual-antenna electromagnetic signal flight paths.

use of a dual-antenna arrangement, as depicted in Figure 18. With this arrangement, it is possible to determine the effective velocity of propagation of the electromagnetic signal in the sea ice, and its effective dielectric constant, irrespective of its changing properties due to temperature or thickness variations. One antenna operates in a transmit-receive mode and the second in a receive-only mode. The antennas are placed a fixed distance apart on the ice and moved as a unit. The effective propagation velocity (V_e) of the signal in the ice is then determined by:

$$V_e = \frac{x}{\sqrt{t_x^2 - t_d^2}} \qquad (9)$$

where x = distance between centers of the two antennas

t_d = vertical travel time from transceiver antenna to and from subsurface interface

t_x = travel time from transceiver antenna to subsurface interface to receive-only antenna (t_x') plus time t_a = air-wave travel time between antennas (Fig. 18).

A more detailed description of the methodology associated with use of a dual-antenna system, and some preliminary results which show that ice thicknesses measured in drill holes and those calculated from eq 9 can be expected to be within 10%, can be found in Kovacs (1977) and Kovacs and Morey (1979b).

With the velocity of the signal thus determined, it is possible to determine sea ice thickness from eq 2 and the average bulk brine volume v of the ice by:

$$v = \frac{0.17 - V_e}{0.0007} \qquad (10)$$

where eq 10 fits the line passing through the data in Figure 17.

Since the mechanical properties of sea ice are a function of its brine volume, it follows that a strength property (σ) of the ice may now be estimated remotely by radio echo sounding. Most strength properties of sea

ice can be represented by an equation of the form:

$$\sigma = a - b\sqrt{v} \qquad (11)$$

where a and b are constants. For example, Vaudrey (1977) found the following relationship from beam test results:

$$\sigma_f = 9.8 - 0.62\sqrt{v} \qquad (12)$$

where σ_f is the flexural strength of sea ice in kg/cm^2. Thus, with the apparent thickness and strength of sea ice known, it follows that the bearing capacity of the ice may also be approximated by analytical methods which are beyond the scope of this report, e.g. see Vaudrey and Katona (1974), Frederking and Gold (1976), Nevel (1978, 1979) and Johnson (1980).

CONCLUSIONS

This study supports previous work (Kovacs and Morey 1978, 1979a) which revealed that for sea ice with a bottom structure in which the horizontal c-axes of the ice crystal platelets are aligned, this ordered bottom structure is an effective polarizer of transverse electromagnetic waves. In short, when a linearly polarized antenna E-field is aligned parallel with the preferred c-axis azimuth, a maximum signal return is received from the ice bottom, but when the antenna is aligned perpendicular to the preferred c-axis orientation, the signal is significantly reduced or eliminated. This effect has been attributed to the ordered arrangement of the brine inclusions, which are believed to create a unique array of lossy, parallel plate waveguides at the ice bottom (Kovacs and Morey 1978). Recent laboratory studies of artificial dielectrics with polarizing effects similar to sea ice support the concept of a sea ice model in which the ice bottom is composed of such an array of waveguides (Morey and Kovacs, in prep.).

In this study additional data are presented which

also verify that the electromagnetic-dependent properties of sea ice vary in the horizontal plane, as does the anisotropy. It is now known that:

1. The average effective bulk dielectric constant, and therefore the average effective velocity of the electromagnetic pulse used in this study, is dependent upon the average bulk brine volume of the sea ice.

2. Sea ice anisotropy may be detected by radio echo sounding measurements made not only on the ice surface but also from an airborne platform.

3. The effective coefficient of reflection from the sea ice bottom:

    a. decreases exponentially with increasing average effective bulk dielectric constant of the ice,

    b. decreases with increasing bulk brine volume, and

    c. is typically one to two orders of magnitude lower than the coefficient of reflection from the ice surface.

4. The losses in sea ice increase "exponentially" with increasing average bulk brine volume.

5. Snow on the ice reduces the voltage amplitude of the electromagnetic wavelet reflected from the ice bottom.

The fundamental relationship between the average bulk brine volume of sea ice and its electrical and strength properties is also discussed. It is shown that, in principle, it should be possible to not only determine sea ice thickness, but also to estimate its strength remotely with the use of a properly designed electromagnetic sounding system.

Implementation of the dual-antenna mode for determining velocity of electromagnetic wave propagation in sea ice may be limited, especially in an airborne mode, to flight altitudes of less than twice the antenna separation, because of inherent limitations in accurately measuring signal flight times of less than about 0.5 ns. Also, this method assumes that most of the electromagnetic anisotropic effects are occurring in the lower 10% of the ice sheet, as postulated in Kovacs and Morey (1979a) and Golden and Ackley (in press). For example, eq 9 is based upon straight ray path propagation in a homogeneous dielectric, which sea ice is not. The propagation distance through sea ice will not be a straight line but will be bent, based upon Snell's law for a material with increasing refractive index (which appears significant for growing winter sea ice only near the ice bottom). Preliminary results with the use of the dual antenna system indicate that ray path bending is not a serious problem (Kovacs 1977). Further evaluation of this is planned.

LITERATURE CITED

Campbell, K.J. and A.S. Orange (1974) A continuous profile of sea ice and fresh water ice thickness by impulse radar. *Polar Record*, vol. 17, p. 31-41.

Frederking, R.M.W. and L. Gold (1976) The bearing capacity of ice covers under static loads. *Canadian Journal of Civil Engineering*, vol. 3, no. 2, p. 288-293.

Golden, K.M. and S.F. Ackley (In press) Modeling anisotropic electromagnetic reflection from sea ice. *Proceedings of International Workshop on the Remote Estimation of Sea Ice Thickness*. Memorial University of Newfoundland, St. Johns.

Johnson, P. (1980) An ice thickness-tensile stress relationship for load-bearing ice. U.S. Army Cold Regions Research and Engineering Laboratory Special Report 80-9.

Kovacs, A. (1977) Sea ice thickness profiling and under ice oil entrapment. *9th Annual Offshore Technology Conference*, Houston, OTC 2949, 547-550.

Kovacs, A. and R.M. Morey (1978) Radar anisotropy of sea ice due to preferred azimuthal orientation of the horizontal c-axes of ice crystals. *Journal of Geophysical Research*, vol. 83, no. 12, p. 6037-6046.

Kovacs, A. and R.M. Morey (1979a) Anisotropic properties of sea ice in the 50–150 MHz range. *Journal of Geophysical Research*, vol. 84, C9, p. 5749-5759.

Kovacs, A. and R.M. Morey (1979b) Remote detection of massive ice in permafrost along the Alyeska Pipeline and the pump station feeder gas pipeline. *Proceedings of the ASCE Specialty Conference on Pipelines in Adverse Environments.* New Orleans, vol. 1, p. 268-280.

Langhorne, P. (In press) Crystal anisotropy in sea ice in the Beaufort Sea. *Proceedings of International Workshop on the Remote Estimation of Sea Ice Thickness.* Memorial University of Newfoundland, St. Johns.

Morey, R.M. and A. Kovacs (In prep.) Time domain reflectometry measurements of sea ice.

Nevel, D.E. (1978) Bearing capacity of river ice for vehicles. CRREL Report 78-3. ADA055244.

Nevel, D.E. (1979) Safe loads computed with a pocket calculator. *Proceedings of Workshop on the Bearing Capacity of Ice Covers, Winnipeg, Manitoba.* National Research Council of Canada, Technical Memorandum No. 123, p. 205-223.

Rossiter, J.R., P. Langhorne, T. Ridings and A.J. Allan (1977) Study of sea ice using impulse radar. *Proceedings, Fourth International Conference on Port and Ocean Engineering under Arctic Conditions.* University of Newfoundland, St. Johns, p. 556-567.

Vaudrey, K.D. (1977) Ice engineering—Study of related properties of floating sea-ice sheets and summary of elastic and viscoelastic analyses. Civil Engineering Laboratory, Naval Construction Battalion Center, Technical Report R860, 81 p.

Vaudrey, K.D. and M.G. Katona (1974) Finite element analysis of floating ice sheets. ASCE National Structural Engineering Meeting, Cincinnati. Preprint 2235, p. 1-27.

Weeks, W.F. and A.J. Gow (1979) Crystal alignment in the fast ice of arctic Alaska. CRREL Report 79-22, 27 p. ADA 077188.

APPENDIX: DATA ANALYSIS PROCEDURES

The radar data were recorded on an analog magnetic tape recorder after down-conversion in the radar receiver. The down-conversion consists of a sampling process, wherein the nanosecond (ns) time frame is converted to a millisecond (ms) time frame for recording and display. A typical scan is shown in Figure A1. The voltage–amplitude vs time plot consists of a series of wavelets representing reflections from the indicated interfaces, e.g. the air/ice interface. The radar receiver contains a time-variable-gain (TVG) circuit which amplifies the signal as time increases. The slope of the TVG function was also recorded on tape. During data analysis, as when the relative peak-to-peak voltage levels of various reflected wavelets were being compared, the effect of the TVG function was removed. Also, part of the field calibration procedure requires calibrating the time base of the radar, using, for example, a length of coaxial cable exactly 10 ns long, or by suspending the antenna a measured distance above a large metal reflector.

A digital signal analyzer was used for laboratory evaluation of the radar data. The same tape recorder used in the field to record the data was used to play the data back through the analyzer. An average of ten
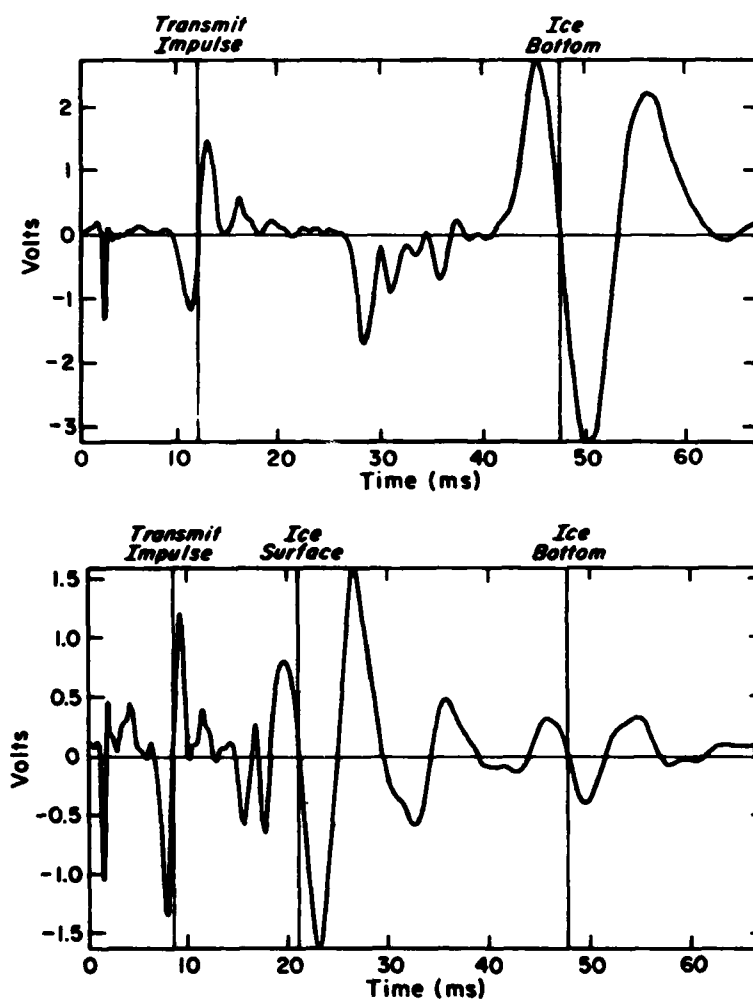

Figure A1. Representative scans obtained from sea ice sounding using impulse radar when antenna was on the ice surface (top) and elevated above the ice surface (bottom).
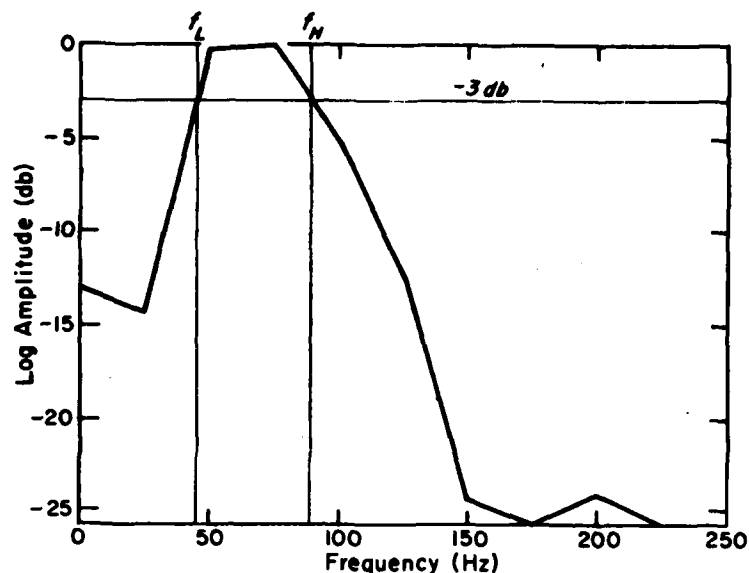
17

Figure A2. Representative reflected wavelet frequency spectrum as generated by digital signal analyzer.

scans was created to reduce the effect of random noise. Movable cursors in the analyzer were positioned at the same point on each wavelet, e.g. the first zero crossing of the air/ice and ice/water interface reflection, and the time difference in milliseconds recorded. A conversion factor was calculated using the 10-ns period between the calibration pulses as displayed on the digital signal analyzer. For this example the pulse period on the analyzer is 33 milliseconds; therefore the conversion factor is $3.3 \times 10^{-2} \div 10^{-8}$, or 3.3×10^6. The conversion factor was used to calculate the two-way travel time in nanoseconds between two wavelets as displayed on the analyzer.

The digital signal analyzer can also calculate the frequency spectrum of a wavelet. This was done by digitizing only the reflected wavelet from a single interface and then calculating the frequency spectrum of that wavelet. The spectrum is displayed as the log amplitude (in db) vs frequency (in Hz), as shown in Figure A2. The −3db points of the spectrum were determined and the center frequency calculated using

$$f_c = (f_H - f_L)/2.$$

For example, f_c in Figure A2 is 67 Hz. This value is then multiplied by the conversion factor to determine the actual center frequency, i.e. $3.3 \times 10^6 \times 67$ Hz=220 MHz.

18

Kovacs, Austin.
  Investigations of sea ice anisotropy, electromagnetic
properties, strength, and under-ice current orientation /
by Austin Kovacs and Rexford M. Morey. Hanover, N.H.: U.S.
Cold Regions Research and Engineering Laboratory; Springfield,
Va.: available from National Technical Information Service,
1980.
  v, 18 p., illus.; 28 cm. (CRREL Report 80-20.)
  Prepared for U.S. Navy, Office of Naval Research and U.S.
Dept. of Commerce, National Oceanic & Atmospheric Adminis-
tration by Corps of Engineers, U.S. Army Cold Regions Research
and Engineering Laboratory.
  Bibliography: p. 16.
  1. Anisotropy. 2. Arctic regions. 3. Electromagnetic.
4. Ocean currents. 5. Sea ice. 6. Strength (mechanics).
I. Rexford Morey. II. United States. III. Army Cold Regions
Research and Engineering Laboratory, Hanover, N.H. IV. Series:
CRREL Report 80-20.